JOURNAL OF SOLID STATE CHEMISTRY 98, 291–300 (1992)

Crystal Chemistry and Magnetism of Neodymium Stannides Including Compounds of the Structural Series RE_nSn_{3n-2}

F. WEITZER, K. HIEBL, AND P. ROGL

Institut für Physikalische Chemie der Universität Wien, A-1090 Wien, Währingerstraße 42, Austria

Received September 16, 1991; in revised form December 2, 1991

DEDICATED TO PROFESSOR DR. H. NOWOTNY ON THE OCCASION OF HIS 80TH BIRTHDAY

The binary system Nd–Sn has been investigated employing X-ray powder techniques and magnetic susceptibility measurements up to 600 K and 6 T. The formation of the compounds Nd_5Sn_3, Nd_5Sn_4, $Nd_{11}Sn_{10}$, NdSn, "Nd_3Sn_5," and $NdSn_3$ has been confirmed. New phases Nd_2Sn_5, Nd_3Sn_7, and $NdSn_2$ have been observed and their crystal structures were found to be isotypic with the structure types of Ce_2Sn_5, Ce_3Sn_7, and $NdSn_2$ ($ZrGa_2$), respectively. Further representatives of the Ce_2Sn_5-, the Ce_3Sn_7-, and the $NdSn_2$-type have been synthesized for La, Pr, and Sm. The lanthanum-containing compounds are diamagnets above 80 K. La_2Sn_5 and $LaSn_2$ become superconducting at 5.4 and 3.6 K, respectively. Pr_2Sn_5 and $PrSn_2$ exhibit metamagnetism, whereas Pr_3Sn_7 is a weak ferromagnet. Nd_5Sn_3 and Nd_3Sn_5 are metamagnets with Neél temperatures T_N = 40 K and T_N = 14 K, respectively, whereas Nd_5Sn_4, $Nd_{11}Sn_{10}$, NdSn, and Nd_3Sn_7 order ferromagnetically at 67, 75, 32, and 10.5 K, respectively. $NdSn_2$, Nd_2Sn_5, and $NdSn_3$ prove to be antiferromagnets at low temperatures. For the new samarium stannides Sm_3Sn_7 and $SmSn_2$, peaks in the susceptibility curves at 20 and 32 K give evidence of antiferromagnetic spin structures.

1. Introduction

Stannides of the rare earth metals have offered a variety of interesting physical properties with respect to magnetic correlations, heavy fermion behavior, and electron–phonon coupling mechanism (*1–9*). This is particularly true for the system Nd–Sn, where interference with magnetic correlations is expected to be stronger than in the homologous cerium stannides (*4*).

The corrosive nature of rare earth stannide compounds in a moist environment has made handling of the alloys quite difficult and up to now has also prevented the construction of reliable constitution diagrams. Enthalpies of formation of rare earth tin alloys have been provided by (*10*), however, no phase diagram calculation was available up to now.

Thus, as a first contribution and as part of a systematic constitutional, structural, and magnetic investigation of the Nd–Mn–Sn system, we herein report on the crystallographic and magnetic characterization of the Nd–Sn binary system, as well as those of novel homologous rare earth stannides.

0022-4596/92 $5.00

2. Experimental

The samples, each with a total weight of ~1 g were prepared by arc-melting proper weights of the constituting elements under high-purity argon on a water-cooled copper hearth. The materials were used in form of ingots as supplied by Auer-Remy GmbH, Germany (Nd–Sm 99.9% pure) and by Merck A.G., Germany (Sn specpure). In order to ensure homogeneity, the samples were remelted several times under as small as possible an electric current in order to minimize weight losses due to vaporization. The reguli were then wrapped in Mo-foil, sealed in evacuated quartz tubes, annealed for 120 hr at 800°C, and quenched by submerging the quartz capsules in cold water.

Due to the high instability of the alloys in a moist environment, handling of the specimens was performed in an argon-filled glove box, ensuring an oxygen level of less than 2 ppm O_2 and ca. 4 ppm H_2O.

Precise lattice parameters and standard deviations were obtained by a least-squares refinement of 114.59-mm Debye–Scherrer or Guinier–Huber X-ray powder data at room temperature employing an internal standard of 99.9999% pure Ge (a_{Ge} = 0.5657906 nm). For protection the powders were sealed in Lindemann capillaries during exposure.

Magnetic measurements have been performed by a SQUID magnetometer down to 2 K. For temperature above liquid nitrogen up to 600 K a Faraday SUS-10 balance was used. All samples were sealed in evacuated and magnetically calibrated quartz tubes to prevent any reaction with residual oxygen and H_2O in the He or Ar atmosphere of the sample chamber of both magnetic devices. The paramagnetic moments μ_{eff} and asymptotic Curie temperatures θ were calculated by a least-squares fit applying a modified Curie–Weiss law.

3. Results and Discussion

3.1. Phase Relations and Structural Chemistry

Room-temperature X-ray phase analysis confirmed formation of the binary compounds reported in literature (see Table I): Nd_5Sn_3, Nd_5Sn_4, $Nd_{11}Sn_{10}$, "NdSn," "Nd_3Sn_5", and $NdSn_3$ (*11–22*). Comparison of observed and calculated X-ray powder intensities, employing the atom parameters reported, revealed satisfactory agreement (see Table II).

Besides these compounds, a series of new phases was observed from alloys annealed at 800°C: $NdSn_2$, Nd_3Sn_7, and Nd_2Sn_5. Whereas the crystal structures of NdSn and Nd_3Sn_5 are still unknown, isotypism between the structure types of Nd_2Sn_5 and Nd_3Sn_7 with the structure types of Ce_2Sn_5 (*23*) and Ce_3Sn_7 (*23*), respectively, was inferred from the close correspondence of their X-ray powder patterns. Using the atom positions refined from single-crystal neutron diffractometry (*23*), X-ray powder intensity calculations are in good agreement with the experimental observation. The structure types of Ce_3Sn_7 and Ce_2Sn_5 were earlier shown to be closely related to $CeSn_3$ and may be obtained by simple shift operations of $CeSn_3$-units generating fivefold or sevenfold supercells, respectively. The shift between two $CeSn_3$ units along $\mathfrak{X} = a/2$ was always accompanied by removal of the two planes of Sn atoms adjacent to the plane of shift.

Applying these principles in order to generate the hitherto unknown threefold supercell directly leads to the structure of $NdSn_2$. Comparison of the calculated X-ray powder pattern with the experimental observation in general is quite convincing and in certain cases is significantly better than employing the atom parameters of the $ZrSi_2$-type, which is observed for all the homolo-

TABLE I

CRYSTALLOGRAPHIC DATA OF SOLID PHASES IN THE BINARY SYSTEM Nd–Sn; DATA FROM LITERATURE

Phase	Structure type	Space group	Unit-cell dimensions (nm)			Comments	Ref.
			a	*b*	*c*		
βNd	W	$Im\bar{3}m$	0.413	—	—		(*11*)
883–863°C							
αNd	αLa	$P6_3/mmc$	0.36579(3)	—	1.17922(5)		(*12*)
<863°C			0.36582	—	1.17966	at 24°C	(*13*)
βSn	Sn(white)	$I4_1/amd$	0.58318(3)	—	0.31819(3)	at 24°C	(*14*)
231.968–13°C							
αSn	$C_{diamond}$	$Fd\bar{3}m$	0.64892	—	—		(*15*)
<13°C							
Nd_5Sn_3	Mn_5Si_3	$P6_3/mcm$	0.9208(8)	—	0.6717(8)		(*16*)
<1640°C			0.9200	—	0.6717		(*17*)
			0.9204	—	0.6725		(*18*)
Nd_5Sn_4	Sm_5Ge_4	*Pnma*	0.814(2)	1.614(1)	0.821(2)		(*16*)
<1500 ± 10°C			0.8222	1.584	0.8376		(*19*)
$Nd_{11}Sn_{10}$	$Ho_{11}Ge_{10}$	*I4/mmm*	1.187	—	1.759		(*19*)
$NdSn_3$	$AuCu_3$	$Pm\bar{3}m$	0.4709	—	—		(*20*)
<1138°C			0.4706	—	—	from kX	(*21*)
			0.4705	—	—	from kX	(*22*)

gous stannides $RESn_2$ with the heavy rare earth members Gd to Lu (*24*). In contrast to the $ZrSi_2$-type, the nonobservance of the (130), (132) reflections and the existence of weak reflections such as (041), (150), etc., is satisfactorily explained in the $NdSn_2$-type. Unit-cell dimensions, crystal symmetry, and atom positions of $NdSn_2$ reveal close correspondence with the structure type of $NdNiGa_2$ (*26*), which is known as a filled up version of the $ZrGa_2$-type (*27*), hence suggesting isotypism between $NdSn_2$ and the $ZrGa_2$-type (*28*). A listing of the crystallographic data for $NdSn_2$ is presented in Table III. Interatomic distances are shown in Table IV. Figure 1 is a representation of the crystal structure of $NdSn_2$ ($NdSn_2$ and hypothetical $ZrSi_2$-type in projection along

TABLE II

CRYSTALLOGRAPHIC DATA OF BINARY ALLOYS Nd–Sn

Nominal composition at.%) Nd–Sn	Treatment	Phase analysis	Structure type	Space group	Unit-cell dimensions (nm)				*c/a*
					a	*b*	*c*	*V*	(*b/a*)
2.5–37.5	Arc	Nd_5Sn_3	Mn_5Si_3	$P6_3/mcm$	0.91981(21)	—	0.67354(22)	0.4935(2)	0.732
5.6–44.4	800°C	Nd_5Sn_4	Sm_5Ge_4	*Pnma*	0.82166(67)	1.58879(278)	0.83809(68)	1.0941(23)	1.934
2.4–47.6	800°C	$Nd_{11}Sn_{10}$	$Ho_{11}Ge_{10}$	*I4/mmm*	1.18440(14)	—	1.76122(99)	2.4707(15)	1.487
0.0–50.0	800°C	NdSn	unknown						
7.5–62.5	800°C	Nd_3Sn_5	unknown						
0.0–65.0	800°C	$NdSn_2$ + Nd_3Sn_5	$NdSn_2$	*Cmmm*	0.44444(14)	1.59436(44)	0.45638(20)	0.3234(2)	3.493
3.4–66.6	800°C	$NdSn_2$	$NdSn_2$	*Cmmm*	0.44404(8)	1.59139(31)	0.45628(8)	0.3224(1)	3.488
0.1–69.9	800°C	Nd_3Sn_7	Ce_3Sn_7	*Cmmm*	0.44990(7)	2.57881(72)	0.45846(8)	0.5317(2)	5.732
3.6–71.4	800°C	Nd_2Sn_5	Ce_2Sn_5	*Cmmm*	0.45688(6)	3.51188(35)	0.46139(6)	0.4703(2)	7.687
0.0–75.0	800°C	$NdSn_3$	Cu_3Au	$Pm\bar{3}m$	0.47061(4)	—	—	0.10423(1)	—

TABLE III

CRYSTALLOGRAPHIC DATA FOR $NdSn_2$

Space group: $Cmmm$-D_{2h}^{19}, No. 65; $Z = 4$
Unit-cell dimensions (X-ray, nm, 295 K):
$a = 0.44404(8)$, $b = 1.59436(44)$, $c = 0.45628(8)$
$b/a = 3.488$, $V = 0.3224(1)$ nm^3
Density: 7.86 Mg/m^3

		Atom parameters		
Atom	Site	x	y	z
Nd	4*i*	0	0.180	0
Sn1	4*j*	0	0.350	$\frac{1}{2}$
Sn2	2*b*	$\frac{1}{2}$	0	0
Sn3	2*d*	0	0	$\frac{1}{2}$

the [001] axis) in comparison with the structure types of Nd_2Sn_5 and Nd_3Sn_7 revealing the building principle of the structural series Ce_nSn_{3n-2} for the combinations of $n = 2, 3, 4$. It is of interest to mention that the end member of this series at $n = 1$ merely represents an orthorhombically distorted CsCl-type. The cubic CsCl-type is well represented among rare earth–monometametal compounds. Members with n higher than $n = 4$ have so far not been encountered at all.

As far as the thermal stability and mode of formation of the binary neodymium stannides are concerned, the congruent melting behavior of Nd_5Sn_3 and $NdSn_3$ is confirmed. In contradiction to the assumed phase diagram (*15*), however, compounds such as

TABLE IV

INTERATOMIC DISTANCES (nm) IN $NdSn_2$

Nd—	2 Nd	0.3145	Sn1—	4 Sn2	0.3183
	4 Sn3	0.3219		4 Sn3	0.3302
	2 Sn3	0.3539		4 Nd	0.3624
	2 Sn1	0.3624			
	2 Sn2	0.3662	Sn3—	4 Nd	0.3219
				2 Sn2	0.3260
Sn2—	4 Sn1	0.3183		2 Sn2	0.3302
	4 Sn3	0.3260		2 Nd	0.3539
	4 Nd	0.3662		3 Sn3	0.3881

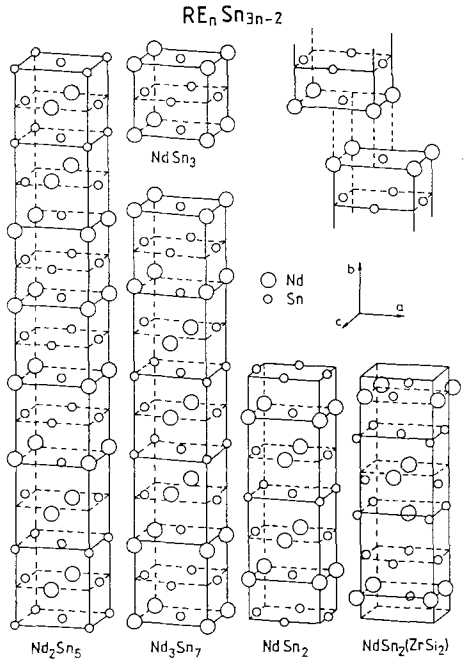

FIG. 1. Comparison of the crystal structures of $NdSn_3$, Nd_2Sn_5, Nd_3Sn_7, and $NdSn_2$ ($NdSn_2(ZrGa_2)$-type and hypothetic $ZrSi_2$-type).

Nd_3Sn_5 and Nd_3Sn_7 were observed to form from invariant reactions involving the liquid phase.

3.2. *Isotypic Compounds RE_nSn_{3n-2}*

In search for further representatives of the above-mentioned structural series RE_nSn_{3n-2}, proper combinations of the light rare earths with tin were arc-melted and heat treated at 800, 600, and 400°C. Novel compounds indeed were revealed in the case of $(La,Pr,Sm)_2Sn_5$, $(La,Pr,Sm)_3Sn_7$, and $(La,Pr,Sm)Sn_2$, which from X-ray powder analysis were found to be isotypic with the structure types expected. Alloys with the nominal compositions "$CeSn_2$" resulted in a heterogeneous two-phase mixture, i.e., no compound formation was observed. A listing of the lattice parameters and crystal data comprising all known compounds of the

TABLE V

CRYSTALLOGRAPHIC DATA OF RARE EARTH STANNIDES $RESn_3$ AND RE_nSn_{3n-2}

Compound	Preparation technique	Structure type	Space group	Unit-cell dimensions (nm)					Ref.
				a	*b*	*c*	*V*	*b*/*c*	
$LaSn_3$	700°C	$AuCu_3$	$Pm\bar{3}m$	0.4769			0.1085		(*21*)
La_2Sn_5	600°C 2w	Ce_2Sn_5	*Cmmm*	0.46233(8)	3.57425(68)	0.46817(8)	0.7336(2)	7.731	*
La_3Sn_7	800°C 5d	Ce_3Sn_7	*Cmmm*	0.45643(12)	2.61558(63)	0.46710(13)	0.5576(3)	5.731	*
$LaSn_2$	800°C 5d	$NdSn_2$	*Cmmm*	0.44267(9)	1.58552(40)	0.45136(8)	0.3168(1)	3.582	*
$CeSn_3$	800°C	$AuCu_3$	$Pm\bar{3}m$	0.47255(6)			0.10552(3)		*
Ce_2Sn_5	800°C 5d	Ce_2Sn_5	*Cmmm*	0.45915(4)	3.52703(79)	0.46498(8)	0.7530(2)	7.682	*
Ce_3Sn_7	800°C 5d	Ce_3Sn_7	*Cmmm*	0.45409(11)	2.57749(57)	0.46235(9)	0.5411(2)	5.676	*
$PrSn_3$	700°C	$AuCu_3$	$Pm\bar{3}m$	0.47159			0.1049		(*21*)
Pr_2Sn_5	800°C 5d	Ce_2Sn_5	*Cmmm*	0.45848(8)	3.51784(57)	0.46338(7)	0.7474(2)	7.673	*
Pr_3Sn_7	800°C 5d	Ce_3Sn_7	*Cmmm*	0.45108(7)	2.58235(52)	0.46037(8)	0.5363(2)	5.725	*
$PrSn_2$	800°C 5d	$NdSn_2$	*Cmmm*	0.44820(11)	1.58973(58)	0.45901(7)	0.3270(2)	3.547	*
$NdSn_3$	800°C	$AuCu_3$	$Pm\bar{3}m$	0.47061(14)			0.10423(1)		*
Nd_2Sn_5	800°C 5d	Ce_2Sn_5	*Cmmm*	0.45688(6)	3.51188(35)	0.46139(6)	0.7403(2)	7.687	*
Nd_3Sn_7	800°C 5d	Ce_3Sn_7	*Cmmm*	0.44990(7)	2.57781(72)	0.45846(8)	0.5317(2)	5.730	*
$NdSn_2$	800°C 5d	$NdSn_2$	*Cmmm*	0.44404(8)	1.59139(31)	0.45628(7)	0.3224(1)	3.584	*
$SmSn_3$	700°C	$AuCu_3$	$Pm\bar{3}m$	0.46866			0.1029		(*21*)
Sm_2Sn_5	800°C 5d	Ce_2Sn_5	*Cmmm*	0.45379(9)	3.49123(85)	0.5861(7)	0.7266(3)	7.693	*
Sm_3Sn_7	800°C 9d	Ce_3Sn_7	*Cmmm*	0.44468(10)	2.59918(61)	0.45229(14)	0.5227(2)	5.747	*
$SmSn_2$	400°C 11d	$NdSn_2$	*Cmmm*	0.44203(13)	1.58399(52)	0.45054(18)	0.3155(2)	3.516	*

Note. An asterisk (*) indicates this work.

RE_nSn_{3n-2} structural series is given in Table V. As seen from the variation of the unit-cell dimension and the volume of the homologues RE_nSn_{3n-2}, the volumes of La_2Sn_5 and $LaSn_2$ are obviously smaller than the corresponding values of the Pr-, or Nd-containing phases. This effect is eventually based on metal defects or Sn-valence instabilities.

3.3. Magnetism

3.3.1. The binary system Nd–Sn. The magnetic properties of the binary system Nd–Sn were studied within the temperature range from 2 to 600 K. The results are listed in Table VI. Figures 2 and 3 show magnetization and inverse susceptibility curves versus temperature.

Nd_5Sn_3 reveals an antiferromagnetic ordering at a Neél temperature T_N = 40 K. The paramagnetic Curie temperature appears to be positive. Hence, the magnetic structure consists of ferromagnetic layers, due to two different crystallographic Nd-sites, which are coupled antiparallel. Similar ferromagnetic sheet formation was observed earlier for $RESn_3$ (*5*). Since the field dependency of the magnetization at 5 K deviates from linearity, a spin flip is likely to occur at high fields.

Nd_5Sn_4, $Nd_{11}Sn_{10}$, NdSn, and Nd_3Sn_7 are ferromagnets with transition points T_c = 67, 75, 32, and 10.5 K, respectively. Nd_5Sn_4 and NdSn are furthermore characterized by a

TABLE VI

MAGNETIC DATA OF THE Nd–Sn BINARY SYSTEM

Compound	T_c (K)	T_N (K)	θ_p (K)	μ_s (μ_B)	μ_{eff} (μ_B)	Ref.
Nd_5Sn_3		40	19.1		3.57	*
Nd_5Sn_4	67		32.8	0.5[a]	3.41	*
$Nd_{11}Sn_{10}$	75		62	1.5	3.40	*
NdSn	32		1.5	0.5[a]	3.56	*
Nd_3Sn_5		14	14.8	1.2	3.64	*
$NdSn_2$		5.1	−8.9		3.69	*
Nd_3Sn_7	10.5		−2.0	0.9	3.65	*
Nd_2Sn_5		3.8	−14.3		3.59	*
$NdSn_3$		4.9	−24.7		3.61	*
		4.7	−22		3.6	(*6*)
		4.6		1.4 ± 0.4		(*7*)

Note. An asterisk (*) indicates this work.

[a] Magnetization/μ_B at H = 3 T.

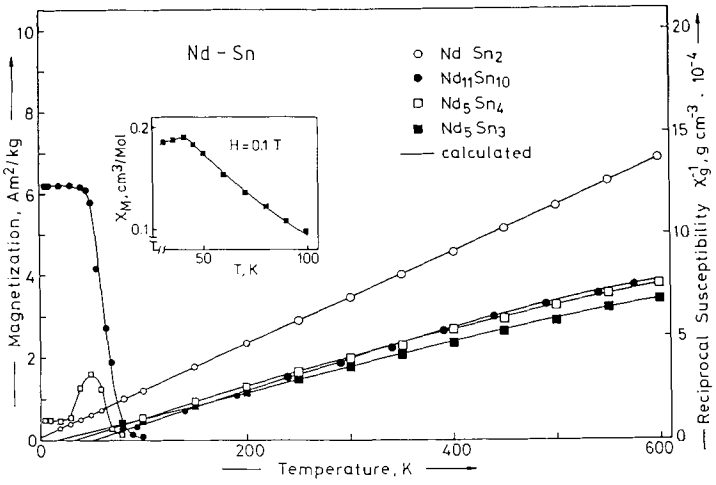

FIG. 2. Magnetization at a magnetic field $H = 0.1$ T and reciprocal susceptibility vs temperature for Nd–Sn alloys. Inset: molar susceptibility vs temperature for Nd_5Sn_3.

strong magnetocrystalline anisotropy. At temperatures as low as 5 K it is not possible to saturate the samples in fields up to 3 T (see Fig. 4) and therefore rather small ferromagnetic moments $\sigma \sim 0.5\ \mu_B$ are found. In the case of $Nd_{11}Sn_{10}$ and Nd_3Sn_7, saturation moments $\mu_s = 1.5\ \mu_B$, and $\mu_s = 0.9\ \mu_B$, which are less than one-half of the free ion moment value $g \cdot J$, are derived, suggesting a noncollinear spin arrangement (canted structure) for both compounds.

The low field (H = 0.1 T) susceptibility curve of Nd_3Sn_5 shows a maximum at T_N = 14 K, indicating an antiparallel spin alignment. However, from the field dependency of the magnetization (see Fig. 4), it is obvi-

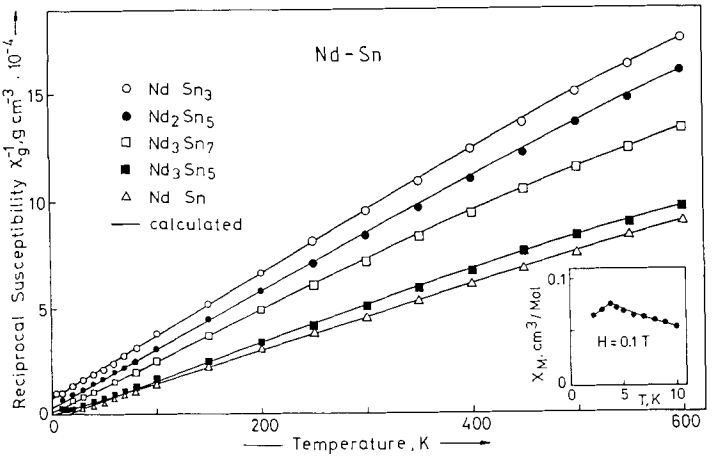

FIG. 3. Reciprocal susceptibility vs temperature for Nd–Sn alloys. Inset: molar susceptibility vs temperature for Nd_2Sn_5.

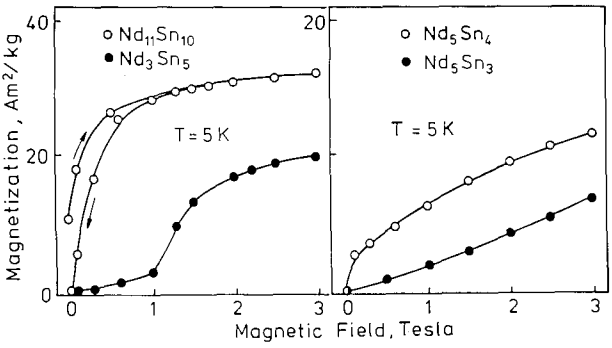

FIG. 4. Magnetization vs field for Nd–Sn alloys at $T = 5$ K.

ous that above a critical field $H_{crit} \approx 1$ T a spin flip takes place and hence a ferromagnetic moment $\mu_s = 1.2\ \mu_B$ is derived.

$NdSn_2$, Nd_2Sn_5, and $NdSn_3$ are found to exhibit antiferromagnetic ordering close to $T = 5$ K. The data for $NdSn_3$ are in good accordance with earlier data (*6*, *7*).

Above liquid-nitrogen temperature all compounds investigated are temperature-dependent paramagnets closely obeying a Curie–Weiss law with effective magnetic moments $\mu_{eff} \sim 3.6\ \mu_B$ owing to the $^4I_{9/2}$ ground state of the neodymium ion. We note that for the tin-rich compounds the paramagnetic Curie temperature changes sign. Assuming the indirect exchange interaction (RKKY-mechanism) as the driving force for the magnetic coupling in these compounds, the type of ordering (i.e., the sign of exchange integral) depends on the oscillatory character of the lattice sum function $\Sigma_i f(2k_F R_i)$, k_F and R_i being the Fermi-wave vector and the position vector of the ith localized spin S_i, respectively. Nevertheless, within each of the particular rare earth rich series RE_nSn_{3n-2} (RE = Cr, Pr, Nd; see below and Ref. (*4*)) the observed θ values do not scale according to the de Gennes factor. Therefore an additional coupling mechanism involving the rare earth $5d$ electrons is suggested.

3.3.2. Isotypic compounds RE_nSn_{3n-2}, RE = La, Pr, Sm. We have also studied the homologous compounds belonging to the structural series RE_nSn_{3n-2}; the magnetic data are given in Table VII and Figs. 5 and 6.

The lanthanum-containing samples (La_2Sn_5, La_3Sn_7, and $LaSn_2$) are diamagnetic in the temperature range investigated. La_2Sn_5 and $LaSn_2$ become superconducting at $T_{sc} = 5.4$ and 3.6 K, respectively, whereas La_3Sn_7 does not undergo a transition down to 2 K. $LaSn_3$ is known as a superconductor at $T_{sc} = 6.25$ K from the literature (*25*). As the average valence electron concentration is nearly constant for these compounds, the volume dependency of the density of states at the Fermi level seems to be more significant for the transition temperature.

Pr_3Sn_7 is a ferromagnet ($T_c = 11.8$ K). The magnetic behavior (see Table VII and Fig. 5) is comparable with isotypic Nd_3Sn_7. The saturation moment $\mu_s = 1\ \mu_B$ again suggests a canted structure.

Pr_2Sn_5 and $PrSn_2$, on the contrary, exhibit metamagnetism. In low magnetic fields the ordering appears to be antiferromagnetic, just as for their Nd homologues. However, when the applied magnetic field is increased above $H_{crit} \sim 1.5$ T, the spin structure changes toward a parallel alignment of the Pr-moments (see Fig. 5). The magnetization

TABLE VII

MAGNETIC DATA OF COMPOUNDS RE_nSn_{3n-2}, RE = La, Pr, Sm

Compound	T_{sc} (K)	T_c (K)	T_N (K)	θ_p (K)	μ_s (μ_B)	μ_{eff} (μ_B)	Ref.
$LaSn_3$	6.25						(25)
La_2Sn_5	5.4		χ_m (80–300 K) = -4.5×10^{-5} cm^3/mole				*
La_3Sn_7	—		χ_m (80–300 K) = -1.7×10^{-4} cm^3/mole				*
$LaSn_2$	3.6		χ_m (80–300 K) = -3.8×10^{-5} cm^3/mole				*
$PrSn_3$			8.6	−8	2.65 ± 0.3	3.42	(6)
Pr_2Sn_5			10.5	11.3	0.7	3.3	*
Pr_3Sn_7		11.8		16.7	1.0	3.6	*
$PrSn_2$			8.4	15.2	1.6	3.1	*
$SmSn_3$			12				(6)
Sm_3Sn_7			20				*
$SmSn_2$			32				*

Note. An asterisk (*) indicates this work.

of $PrSn_2$ tends to saturize only at rather high fields of $H > 5$ T, and a magnetic moment $\mu_s = 1.6\ \mu_B$ is deduced. The paramagnetic moments for both compounds appear to be slightly reduced, as observed earlier in case of the low temperature antiferromagnet $PrSn_3$ (6). As the moment calculations were generally done for temperatures $T > 80$ K, the influence of crystal fields can be neglected and thus the moment reduction might arise from a partial delocalization of the praseodymium $4f$ electrons. The deflection of the low-temperature susceptibility data from the calculated linear part of the $1/\chi$ curve is attributed to a crystalline field split ground state.

Finally, the susceptibility curves (inset Fig. 6) of both compounds Sm_3Sn_7 and $SmSn_2$ show rather broad cusp-like peaks at $T_N = 20$ K and $T_N = 32$ K. $SmSn_3$, on the contrary, shows a sharp peak at 12 K (6) and the samarium moments are oriented

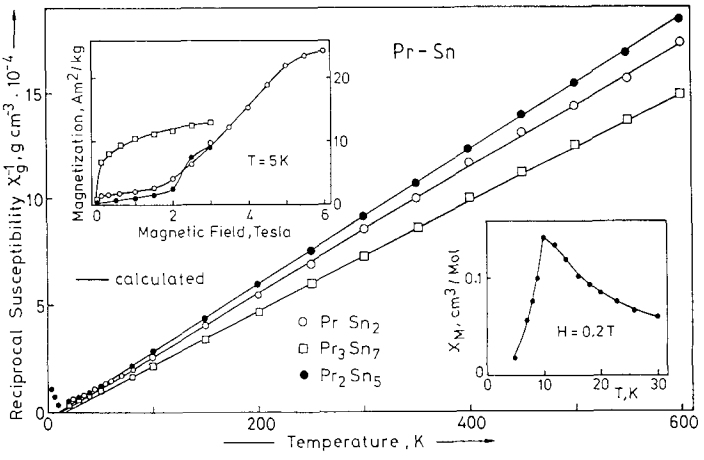

FIG. 5. Reciprocal susceptibility vs temperature for Pr–Sn alloys. Upper inset: magnetization vs magnetic field for Pr–Sn alloys. Lower inset: molar susceptibility vs temperature for Pr_2Sn_5.

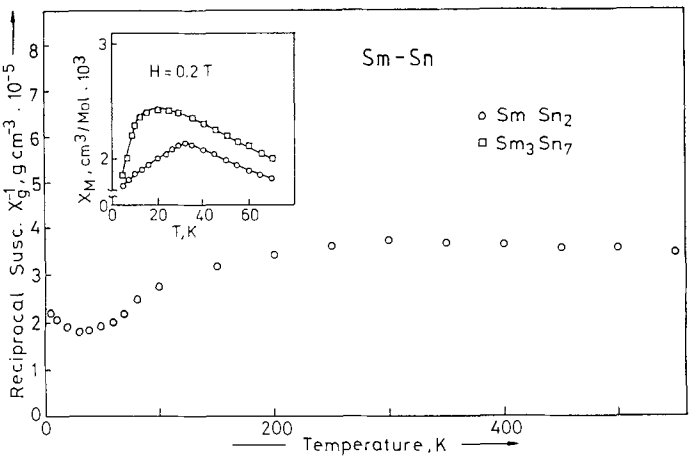

FIG. 6. Reciprocal susceptibility vs temperature for $SmSn_2$. Inset: molar susceptibility vs temperature for Sm_3Sn_7 and $SmSn_2$.

along the |111| directions, arranged antiparallel in successive (100) planes (*5*). Thus, it is concluded that the antiferromagnetic structures of the above two compounds are rather complex; helical spin arrangements along one of the crystallographic axes, such as observed earlier in case of $GdSn_3$ (*5, 6*) are likely. The paramagnetism of both phases is characterized by a Van Vleck type due to closely spaced multiplets (see Fig. 6).

Acknowledgments

This research was sponsored through the European Community as a SCIENCE Project ERB SCI*CT 910738. P.R. expresses his gratitude to the Hochschuljubiläumsstiftung der Stadt Wien for the KD-530 microdensitometer and the MNT-306 microbalance.

Thanks are furthermore due to the Österreichische Nationalbank for the Guinier Huber System (Grant 3519) and the high-temperature camera (Grant 3804). K.H. is grateful to the CNRS and the Austrian Academy of Sciences for a two-month fellowship in Rennes, France.

References

1. M. NIKSCH, I. KONROUDIS, W. ASSMIRS, AND B. LÜTHE, *J. Magn. Magn. Mater.* **47 & 48,** 297 (1985).
2. J. SAKURAI, H. KAMIMURA, AND Y. KOMURA, *J. Magn. Magn. Mater.* **76 & 77,** 287 (1988).
3. F. STEGLICH, *J. Phys. Chem. Solids* **50,** 225 (1989).
4. F. WEITZER, K. HIEBL, AND P. ROGL, *J. Less-Common Met.* **175,** 331 (1991).
5. J. P. SANCHEZ, J. M. FRIEDT, G. K. SHENOY, A. PERCHERON, AND J. C. ACHARD, *J. Phys. C* **9,** 2207 (1976).
6. T. TSUCHIDA AND W. E. WALLACE, *J. Chem. Phys.* **43,** 3811 (1965).
7. P. LETHUILLIER, J. PIERRE, K. KNORR, AND W. DREXEL, *J. Phys.* **36,** 329 (1975).
8. J. M. HASTINGS, L. M. CORLISS, W. KUNNMANN, R. THOMAS, J. BEGUM, AND P. BAK, *Phys. Rev. B* **22,** 1327 (1980).
9. Z. KLETOWSKI, *Solid State Commun.* **62,** 745 (1987).
10. C. COLINET, A. PASTUREL, A. PERCHERON-GUEGAN, AND J. C. ACHARD, *J. Less-Common Met.* **102,** 167 (1984).
11. F. H. SPEDDING, J. J. HANAK, AND A. H. DAANE, *J. Less-Common Met.* **3,** 110 (1961).
12. B. A. ROGERS AND D. F. ATKINS, *J. Met.* **7,** 1034 (1955).
13. K. A. GSCHNEIDER, JR., AND L. EYRING, "Handbook on the Physics and Chemistry of Rare Earths," Vol. 1, p. 216. North-Holland, Amsterdam (1978).
14. V. T. DESPHANDE AND D. P. SIRESHMUKH, *Acta Crystallogr.* **14,** 355 (1961).
15. T. B. MASSALSKI, "Binary Alloy Phase Diagrams," 2nd ed., Vol. 1, p. 1112, ASM International, Materials Park, OH (1990).
16. V. N. EREMENKO, A. M. KHARKOVA, AND I. M. OBUSHENKO, *Dopov. Akad. Nauk. Ukr. RSR* **12,** 1134 (1978).

17. A. PALENZONA AND F. MERLO, *Atti Accad. Naz. Lincei Rend. Cl. Sci. Fis. Mat. Nat.* **40,** 617 (1966).
18. W. JEITSCHKO AND E. PARTHÉ, *Acta Crystallogr.* **22,** 551 (1967).
19. M. L. FORNASINI AND F. MERLO, *Atti Accad. Naz. Lincei Rend. Cl. Sci. Fis. Mat. Nat.* **50,** 186 (1971).
20. A. F. RUGGIERO AND G. L. OLCESE, *Atti. Accad. Naz. Lincei Rend. Cl. Sci. Fis. Mat. Nat.* **37,** 169 (1964).
21. I. R. HARRIS AND G. V. RAYNOR, *J. Less-Common Met.* **9,** 7 (1965).
22. A. IANDELLI, "The Physical Chemistry of Metallic Solutions and Intermetallic Compounds," Paper No. 3F, H.M.S.O., London (1959).
23. J. X. BOUCHERLE, F. GIVORD, P. LEJAY, J. SCHWEIZER, AND A. STUNAULT, *Acta Crystallogr. Sect. B: Struct. Sci.* **B44,** 377 (1988).
24. A. IANDELLI AND A. PALENZONA, *Atti Accad. Naz. Lincei Rend. Cl. Sci. Fis. Mat. Nat.* **40,** 623 (1966).
25. B. STALINSKY, Z. KLETOWSKI, AND Z. HENKIE, *Phys. Status Solidi A* **19,** K165 (1973).
26. YU. M. GRIN AND YU. P. YARMOLYUK, *Dopov. Akad. Nauk. Ukr. RSR, Ser. A,* 69 (1982).
27. M. PÖTZSCHKE AND K. SCHUBERT, *Z. Metallkd.* **53,** 475 (1962).
28. E. PARTHÉ, private communication.